Phase-shifter calibration and error detection in phase-shifting applications: a new method

Bernd Gutmann and Herbert Weber

The phase-shifting technique is used in optical metrology to evaluate the local phase of a fringe pattern. Accurate calibration of the shifting device is often essential but sometimes hardly possible because of deviations of the fringe pattern from the ideal sinusoidal shape and because of a nonconstant phase shift between consecutive frames. We introduce a new technique for calculating the phase shift between frames even in the presence of high noise and nonsinusoidal fringe patterns. In addition, this technique permits the identification of different error sources such as low signal-to-noise ratio, higher harmonics contained in the fringe pattern, and nonconstant phase shift. © 1998 Optical Society of America

OCIS codes: 110.4280, 120.2650, 120.3940, 120.5050.

1. Introduction

In optical metrology many different methods provide measurement information by the use of fringe patterns. Depending on the application and the measurement task, fringes can store information about, e.g., contour, deformation, stress, and index of refraction.[1,2] These fringe patterns can be recorded by a CCD camera and processed by a computer to yield the desired information. A simple mathematical representation of the recorded fringe intensity at point (x, y) is given by

$$I(x, y) = I_0(x, y)[1 + \gamma(x, y)\cos \phi(x, y)],$$
$$0 \le \gamma(x, y) \le 1,$$

with the local background intensity $I_0(x, y)$, the fringe visibility $\gamma(x, y)$, and the phase $\phi(x, y)$, which contains the desired measurement information.

There are several methods for extracting the phase from the fringes that satisfy various demands for speed, accuracy, and complexity.[1,2] The phase-shifting or phase-stepping technique is one way to retrieve the phase with high accuracy. With this technique several images of the fringe patterns (i.e.,

frames) are recorded and the phase between two consecutive images is shifted by an amount α (i.e., the shift angle) through one of several means (e.g., piezo-mounted mirrors in laser-interferometric applications or linear translation stages in fringe-projection applications). Frame n is then represented by

$$I_n(x, y) = I_0(x, y)\{1 + \gamma(x, y)\cos[\phi(x, y) + (n - 1)\alpha]\},$$

$$(1)$$

with $n = 1, 2, \ldots , N$ and $N \in IN, N \ge 3$.

As Eq. (1) contains three unknown variables at each point (x, y), at least three frames are required for evaluation of the phase. Depending on the shift angle α and on the number of images N, there is a formula to calculate the phase at each point. The choice of α and N depends on requirements such as speed of the algorithm, sensitivity to shift errors and higher harmonics, and accuracy of the retrieved phase. By using the addition theorems, one can derive these formulas for a fixed value of α, assuming a harmonic shape of the fringes. If these assumptions are violated, systematic errors occur in the evaluation of the phase.

Meanwhile, various algorithms have been developed that deal with error sources such as nonconstant shift angle and nonsinusoidal fringes (see, e.g., Ref. 3). But the commonest and easiest formulas to implement still have limitations with respect to the deviation of the actual shift angle from the theoretical value. Therefore a sufficiently exact calibration of the shifting device is indispensable for measurements with high accuracy. Several techniques to obtain an unknown phase shift from the intensity patterns have been developed. If, for example, five intensity measurements

The authors are with the Institut für Mechanische Verfahrenstechnik und Mechanik, Bereich Angewandte Mechanik, Universität Karlsruhe, 76128 Karlsruhe, Germany. B. Gutmann's e-mail address is bernd.gutmann@ciw.uni-karlsruhe.de.

are taken with an unknown but constant shift angle α between two consecutive frames, the phase shift at each point (x, y) can be calculated by[4]

$$\cos \alpha = \frac{1}{2} \frac{I_5(x, y) - I_1(x, y)}{I_4(x, y) - I_2(x, y)}. \qquad (2)$$

Because of noise and other errors, the retrieved value for α will not be constant for all points (x, y) within the measurement field; thus $\alpha = \alpha(x, y)$. Some applications now determine the shift angle from the mean value of $\alpha(x, y)$. This method does yield good results as long as the spread of the distribution of $\alpha(x, y)$ is approximately symmetric.

Another method uses the histogram of $\alpha(x, y)$ within the measurement field. As the intensity values I_n are discrete, $\alpha(x, y)$ turns out to be discrete, too. Thus it is possible to calculate a histogram that shows the frequencies of all values of $\alpha(x, y)$ within the measurement field; therefore the shift angle can also be evaluated by its maximum appearance.[5] In the ideal case the histogram shows a definite peak with a small and symmetric spread. Spatial variations of the phase shift result in irregular shape and spread of the histogram. Considering the variety of shifting devices and applications, several error sources exist that will influence the shape of the histogram severely and prevent an evaluation of the shift angle by use of the maximum frequency only. Typical errors are

- High additive intensity noise (electronic noise).
- Phase noise (speckle noise).
- Nonlinearities of the shifting device (e.g., hysteresis of a piezo translator).
- Random errors of the shifting device (e.g., mechanical problems).
- Spatial inhomogenities of the shifting device (e.g., tilt of a piezo translator).
- Higher harmonics of the fringes (e.g., by insufficient defocusing of the projected rectangular-profile fringes).
- Numerical problems through quantization of the intensity values.

In the following sections we illustrate the influence of errors on the shape of the peak in the histogram. A tool is provided that will help in identifying the above error sources in an application and at the same time in evaluating the shift angle with high degrees of accuracy and repeatability.

2. Identification of Error Sources and Evaluation of the Shift Angle by Means of Lattice-Site Representation

A. Principle

The new method is based on an alternative representation of the results of Eq. (2). Instead of counting the frequencies of shift angles, one counts the frequency $H(M, Z)$ of each combination of numerator $Z = (I_5 - I_1)$ and denominator $M = 2G = 2(I_4 - I_2)$ and represents them by a corresponding gray level in a two-dimensional diagram with Z as the ordinate and M as
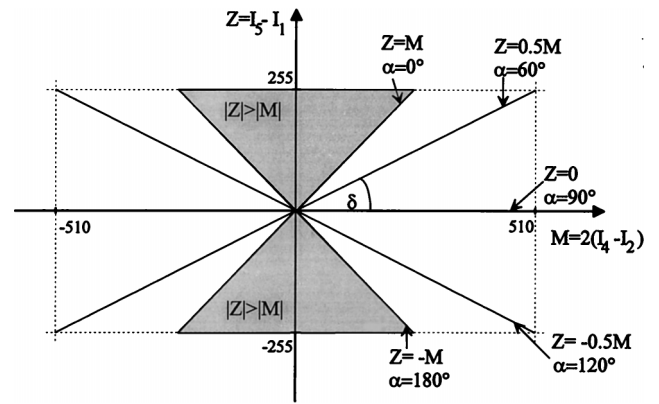

Fig. 1. Coordinate system for the lattice-site representation. The rectangle denotes the range of numerator and denominator for 256 gray levels. The origin straight lines represent lattice sites with equal shift angles α.

the abscissa. Figure 1 illustrates the range of possible points in the diagram and their relation to the shift angle α. The quantization of the intensity values I_n and their limitation to 8 bits causes the numerator to be limited to the integer values $[-255, -254, \ldots, -1, 0, 1, \ldots, 254, 255]$ and the denominator to the integer values $[-510, -508, \ldots, -2, 0, 2, \ldots, 508, 510]$. Thus valid positions in the diagram are restricted to isolated points. Another limitation is that Eq. (2) requires that

$$|\cos \alpha| \leq 1 \Rightarrow |I_5 - I_1| \leq 2|I_4 - I_2| \Rightarrow |Z| \leq |M|.$$

As, for a given shift angle α, the ratio between Z and M is fixed, all points that represent α lie upon an origin straight line that includes an angle δ with the M axis (Fig. 1). The relation between α and δ is given by

$$\alpha = \arccos(\tan \delta). \qquad (3)$$

Shown in Fig. 1 are lines that represent shift angles of $\alpha = 0°$ ($Z = M$), $\alpha = 60°$ ($Z = 0.5M$), $\alpha = 90°$ ($Z = 0$), $\alpha = 120°$ ($Z = -0.5M$), and $\alpha = 180°$ ($Z = -M$).

We call valid positions in this diagram lattice sites. Thus we refer to this representation as the lattice-site representation. To illustrate its meaning for the identification of error sources and the evaluation of the shift angle, we apply it first to computer-generated fringe patterns.

B. Simulation of Noisy Fringe Patterns of Different Shapes

We used Eq. (1) as a basis to simulate fringe patterns that would be modified by different error sources. To achieve a realistic simulation we altered $\phi(x, y)$ in both dimensions [Fig. 2(a)]:

$$\phi(x, y) = (2\pi x/\lambda_x) + \cos(2\pi y/\lambda_y). \qquad (4)$$

The central-limit theorem states that, if the contributions of different noise sources to the overall noise
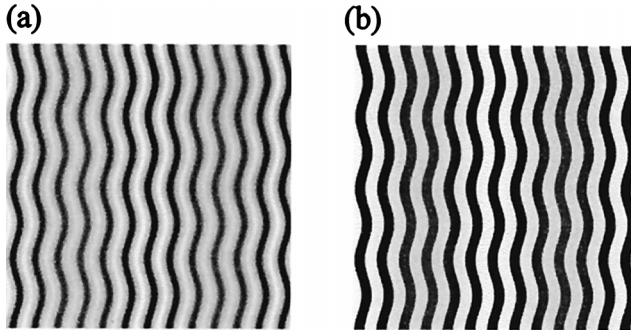
Fig. 2. Simulated fringe patterns with varying fringe visibility: (a) sinusoidal fringes and (b) a Ronchi grating.

are of the same dimension, one can describe the probability density of the noise by the normal distribution

$$f_{\Delta I}(\Delta I) = \frac{1}{\sqrt{2\pi}\sigma_I} \exp\left(-\frac{\Delta I^2}{2\sigma_I^2}\right).$$

Using Eq. (1), we can describe fringe patterns with additive intensity noise ΔI with standard deviation σ_I and zero mean by

$$I_n^*(x, y) = I_n(x, y) + \Delta I(\sigma_I) \qquad (5)$$

and the signal-to-noise ratio (SNR) by

$$\mathrm{SNR}_{\mathrm{dB}} = 20 \log_{10}\left(\frac{I_0\gamma}{\sqrt{2}\sigma_I}\right).$$

In addition to having errors that are due to intensity noise, realistic fringe patterns can also differ from the ideal sinusoidal shape given by Eq. (1) through higher harmonics. Fringes that contain higher harmonics are a typical effect within fringe-projection applications if the projection system uses rectangular fringes that are not defocused sufficiently. Thus simulating a more-or-less defocused grating with a rectangular transmission function (Ronchi grating) provides a tool for the investigation of a very important error source in optical metrology. Defocusing is due to the optical transfer function $\mathrm{OTF}(k)$ of the projection system, as it decreases rapidly for high frequencies k, depending on the adjusted blur. To simulate a defocused Ronchi grating, we chose $\mathrm{OTF}(k)$ simply as

$$\mathrm{OTF}(k) = \exp\left(-\frac{k^2}{2\sigma_k^2}\right).$$

With $\mathbf{k} = \mathrm{grad}\ \phi(x, y)$ and by using Eq. (4), we obtain

$$k^2 = 4\pi^2/\lambda_x^2 + (4\pi^2/\lambda_y^2)\sin^2(2\pi y/\lambda_y).$$

A Ronchi grating can then be simulated by

$$R[\phi(x, y)] = \frac{1}{\Omega} \sum_{m=1}^{Q+1} \exp\left(-\frac{m^2 k^2}{2\sigma_k^2}\right)$$
$$\times \mathrm{sinc}(m\pi/2)\cos[m\phi(x, y)], \qquad (6)$$

with the scaling factor

$$\Omega = \sum_{m=1}^{Q+1} \exp\left(\frac{-m^2 k^2}{2\sigma_k^2}\right)\mathrm{sinc}(m\pi/2);$$

thus $-1 \leq R[\phi(x, y)] \leq 1$. The shape of the fringes depends on σ_k and Q. Small values of σ_k rapidly cut off higher harmonics, resulting in sinusoidal fringes; for higher values of σ_k the fringes tend toward a rectangular shape.

The number of higher harmonics that contribute to the fringe pattern is given by Q. It can be chosen small if σ_k is small too, but it should be chosen sufficiently large, e.g., $Q > 10$, if realistic undefocused Ronchi gratings are required [Fig. 2(b)].

Thus, from Eqs. (1) and (4)–(6), phase-shifted noisy fringe patterns will be simulated by

$$I_n(x, y) = I_0(x, y)\{1 + \gamma(x, y)R[\phi(x, y) + (n - 1)\alpha]\}$$
$$+ \Delta I(\sigma_I). \qquad (7)$$

C. Frequency Distribution of the Lattice Sites

The distance of a lattice site to the origin is given by

$$r^2 = Z^2 + M^2 = (I_5 - I_1)^2 + 4(I_4 - I_2)^2.$$

Using Eq. (1), we find that

$$I_5 - I_1 = -2I_0\gamma \sin(\phi + 2\alpha)2 \sin\alpha \cos\alpha,$$

$$I_4 - I_1 = -2I_0\gamma \sin(\phi + 2\alpha)\sin\alpha.$$

Thus, if I_0, γ, and α in Eq. (1) are fixed, the distance of the corresponding lattice site to the origin depends on $\phi(x, y)$ by

$$r^2 = \{4I_0\gamma \sin\alpha \sin[\phi(x, y) + 2\alpha]\}^2(1 + \cos^2\alpha). \qquad (8)$$

The frequency distribution $f_r(r)$ of the distance r for a given probability density $g_\phi(\phi)$ of the phase values can be evaluated from
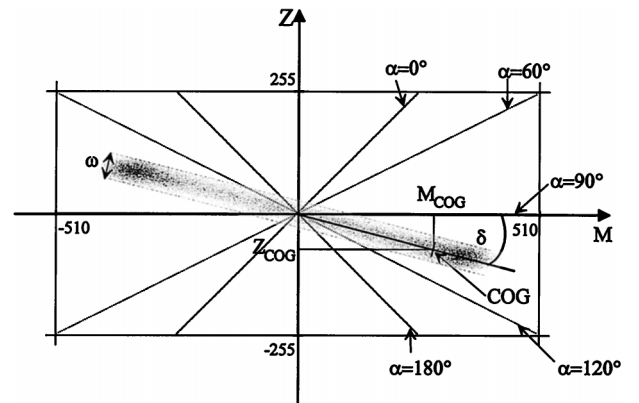
$$f_r(r)\mathrm{d}r = g_\phi(\phi)\mathrm{d}\phi,$$

Fig. 3. Lattice-site representation of shift angles for simulated fringe patterns with additive intensity noise from Eq. (7) with $\alpha = 105°$, $Q = 0$, $\gamma = 0.75$, $I_0 = 127$, and $\sigma_I = 10$ (SNR, 16.6 dB). Two highly populated cores with width ω are shown. The line through the center of gravity includes an angle δ with the M axis.
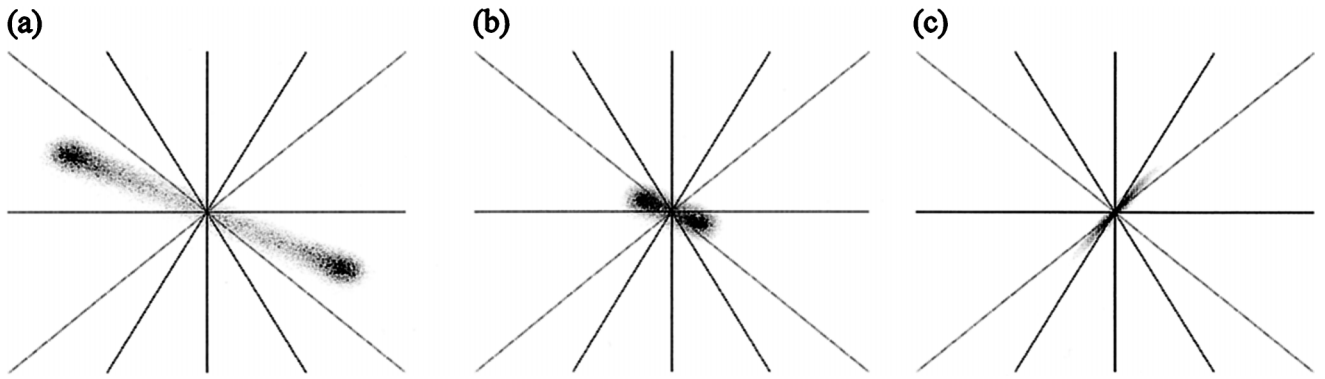
Fig. 4. Influence of noise on cores and tails in the lattice-site representation: (a), (b) Simulated fringe patterns from Eq. (7) with $\alpha = 105°$, $Q = 0$, $\gamma = 0.75$, and $\sigma_I = 10$. (a) $I_0 = 127$; SNR, 16.6 dB. (b) $I_0 = 30$; SNR, 4.0 dB. (c) Real measurement of a phase-shifted electronic speckle-pattern interferometry pattern with a low SNR, shifted by 50°.

which yields

$$f_r(r) = g_\phi(\phi)\left(\frac{dr}{d\phi}\right)^{-1}.$$

After normalization, we find that

$$f_r(r) = \{\pi[(4I_0\gamma \sin \alpha)^2(1 + \cos^2 \alpha) - r^2]^{1/2}\}^{-1}, \quad (9)$$

which yields a higher population of the lattice sites for bigger distances r to the origin.

Figure 3 shows an example of a simulated sinusoidal fringe pattern with low additive intensity noise. The shift angle between consecutive frames was chosen to be $\alpha = 105°$. Gray levels correspond to the relative frequency of a given combination of Z and M within the measurement field. Dark values indicate a high frequency, whereas white means no population at all. From Eq. (9), the population increases for an increasing distance r, revealing two highly populated cores and two lower-populated tails that extend from the cores to the origin. The spread of the population is due to the additive noise. The meanings of ω and the center of gravity (COG) are described below.

D. Calculation of the Shift Angle by the Center-of-Gravity Method

A simple method for calculating the shift angle by means of the lattice-site representation is to look for the lattice site with the highest frequency. We found, however, that this method is not reliable in the presence of shift errors, higher harmonics, and other error sources. The task was to find a reliable way to compute the shift angle without using complicated methods in image processing, so the algorithm would be fast and easy to implement.

We found that the COG of $H(M, Z)$ on either side of the Z axis gives accurate results for the shift angle. The COG of a mass distribution is given by

$$\mathbf{r}_s = \frac{\sum_i m_i \mathbf{r}_i}{\sum_i m_i}.$$

If the frequency $H(M, Z)$, $M = 2G$, of a lattice site is identified with the mass, we obtain

$$M_{COG} = \frac{\left[\sum_{G=1}^{255}\sum_{Z=-255}^{255} 2G \times H(2G, Z)\right]}{\left[\sum_{G=1}^{255}\sum_{Z=-255}^{255} H(2G, Z)\right]},$$
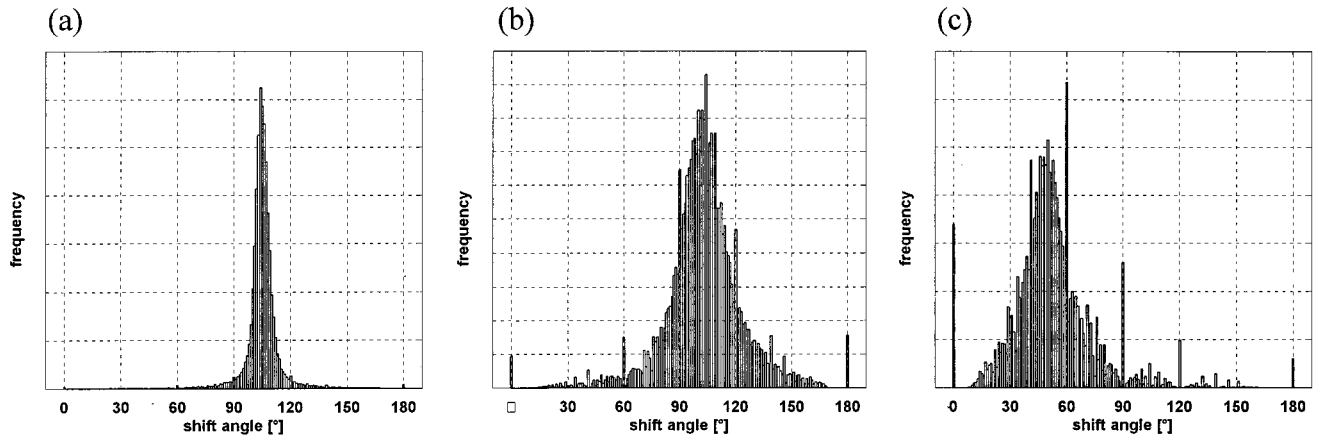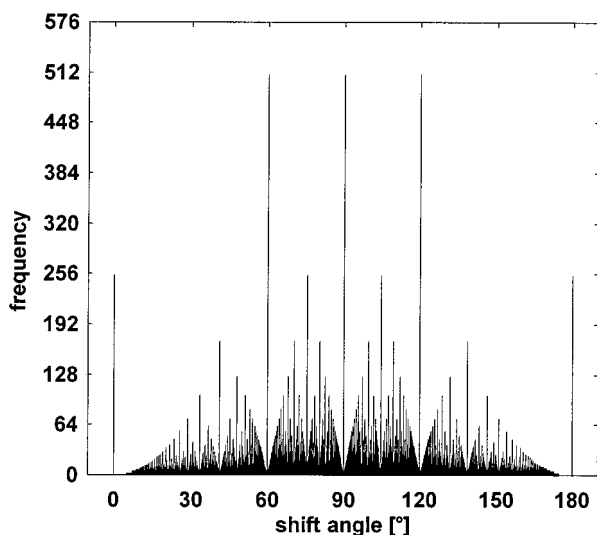

Fig. 5. Histograms for the fringe patterns used in Fig. 4.

Table 1. Shift-Angle Calculation by Several Methods for Simulated Fringe Patterns with Additive Intensity Noise [from Eq. (7) with $Q = 0$, $\gamma = 0.75$, and $\alpha = 105°$ for All Patterns] and for a Real Phase-Shift ESPI Measurement Shifted by $\alpha = 50°$

Parameter and Method	Simulation 1	Simulation 2	Simulation 3	Simulation 4	Phase-Shift ESPI
σ_I	5	10	10	10	
I_0	127	127	50	30	
SNR (dB)	22.6	16.6	8.5	4.0	
α calculated by COG ($M > 0$)	104.9°	104.9°	104.5°	103.4°	48.6°
α calculated by COG ($M < 0$)	105.1°	105.1°	104.2°	103.4°	48.9°
α calculated by lattice site with maximum frequency	104.5°	105.6°	99.8°	105.5°	No result, $\lvert Z_{MAX}\rvert > \lvert M_{MAX}\rvert$
α calculated by maximum histogram value	106°	105°	105°	105°	60°
Mean value of $\alpha(x, y)$ within the measurement field	104.9°	104.8°	104.2°	103.0°	52.8°

$$Z_{\mathrm{COG}} = \frac{\left[\displaystyle\sum_{G=1}^{255}\sum_{Z=-255}^{255} Z \times H(2G, Z)\right]}{\left[\displaystyle\sum_{G=1}^{255}\sum_{Z=-255}^{255} H(2G, Z)\right]},$$

for the coordinates of the COG of the frequency distribution for positive values of M. The COG on the left-hand side of the M axis can be calculated similarly. Using

$$\alpha = \arccos\frac{Z_{\mathrm{COG}}}{M_{\mathrm{COG}}}$$

yields an accurate value for the shift angle α. In most cases the results of the two COG's differ only within 0.5°.

Because of the influence of various error sources (e.g., noise), the lattice-site representation might also yield a population in areas with $\lvert Z\rvert > \lvert M\rvert$. These values cannot be evaluated by Eq. (2) and must therefore be excluded if α is calculated by the mean value. The COG method, however, makes use of these values, as the limitation $\lvert Z\rvert \leq \lvert M\rvert$ applies only to the

coordinates of the COG. Thus the results of the COG method are more exact than those of the mean value of α, especially in the presence of significant errors. Figure 3 shows an origin straight line through the COG, including an angle δ with the M axis. The relation between δ and α is given by Eq. (3). The influence of various error sources on the calculation of α and on the shapes of tails and cores in the lattice-site representation is discussed below.

E. Influence of a Low Signal-to-Noise Ratio

Figures 4 and 5 illustrate the influence of a low SNR on both lattice-site representations and histograms for two simulated fringe patterns and a phase-shifted electronic speckle-pattern interferometry (ESPI) measurement. Experiments showed that the influence of phase noise on the lattice-site representation is similar to the influence of additive intensity noise.

The histograms clearly show how the peak of the frequency distribution broadens, whereas noise increases. Isolated peaks occur that gradually surpass the actual peak, thus preventing the histogram from being evaluated correctly. In addition, the histogram of the ESPI measurement [Fig. 5(c)] shows structures (e.g., the frequency distribution of shift angles from 90° to 120°) that do not correspond to the

Fig. 6. Number of combinations of Z and M that yield the same shift angle α.
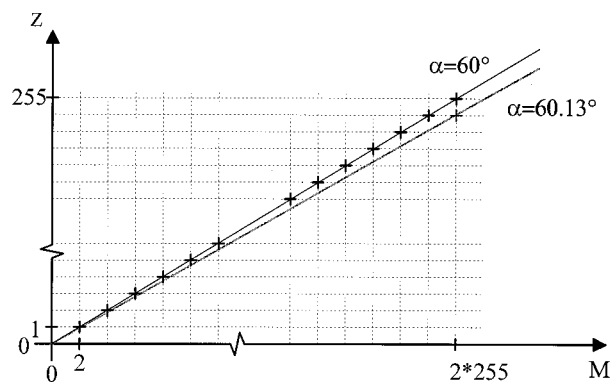
Fig. 7. Illustration of the level of degeneracy for $\alpha = 60°$ and $\alpha = 60.13°$. The line for $\alpha = 60°$ contains 254 possible combinations of integer values of Z and M (lattice sites), whereas there is only one combination (i.e., [510, 254]) that yields $\alpha = 60.13°$.
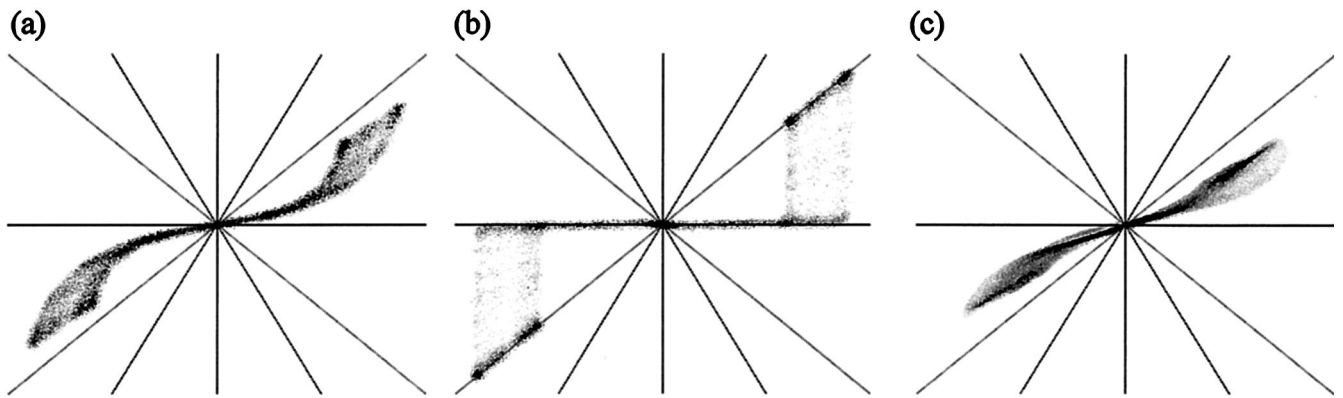
Fig. 8. Influence of higher harmonics on cores and tails in the lattice-site representation: (a), (b) Simulated fringe patterns from Eq. (7) with $\alpha = 72°$, $I_0 = 127$, γ varying from 0.55 to 0.95, $\sigma_I = 3$, and $Q = 10$. (a) $\sigma_k = 0.7$ and (b) $\sigma_k = 2.0$. (c) Real measurement in a projected-fringe application with a nondefocused Ronchi grating, shifted by 72°.

frequency distribution of the phase noise, an effect that can be explain by the intensity quantization (Subsection 2.F).

In the lattice-site representation the SNR has an influence on both the widths ω of tails and cores and the distance of the cores to the origin. The width ω increases with increasing σ_I, whereas the distance of the cores increases with increasing $I_0\gamma$.

The results of several methods for evaluating the shift angle are given in Table 1. All methods yield accurate results in the case of simulated patterns. Using the maximum of the histogram seems to be the most successful method, but this is so because we restricted the histogram to integer values in steps of 1°. Therefore the apparent accuracy is due to low resolution. The ESPI measurement, however, reveals that only the mean value of $\alpha(x, y)$ and the COG's of the lattice-site representation provide reliable results.

F. Influence of the Intensity Quantization

The histograms shown in Figs. 5(b) and 5(c) show isolated peaks at values of 0°, 60°, 90°, 120°, and 180° that increase with decreasing SNR. These peaks can surpass the peak of the actual shift angle, pre-venting the histogram from being evaluated by its maximum frequency.

We can show similar effects by counting the number of possible occurrences of values of α. As the analog sensor signal is digitized into a range of 256 gray levels, the number of possible values for Z and M is limited to $[-255, -254, \ldots, 254, 255]$ and $[-510, -508, \ldots, 508, 510]$, respectively. If we now calculate α by using Eq. (2) for all possible values of Z and M within their individual ranges, some values of α appear more frequently than others (Fig. 6). We call the number of combinations of Z and M that yield the same value for α the level of degeneracy. Figure 6 shows highly degenerate shift angles at 60°, 90°, and 120° (each has 510 possibilities) and at 0° and 180° (254 possibilities). It can also be seen that these values are always neighbors of shift angles with a low degree of degeneracy. These shapes also appear in histograms of fringe patterns with very low SNR's [cf. Figs. 5(c) and 6].

The occurrence of these peaks can be explained through the effects of quantization of the intensity values I_n. Figure 7 illustrates the quantization effect when the lattice-site representation is used for
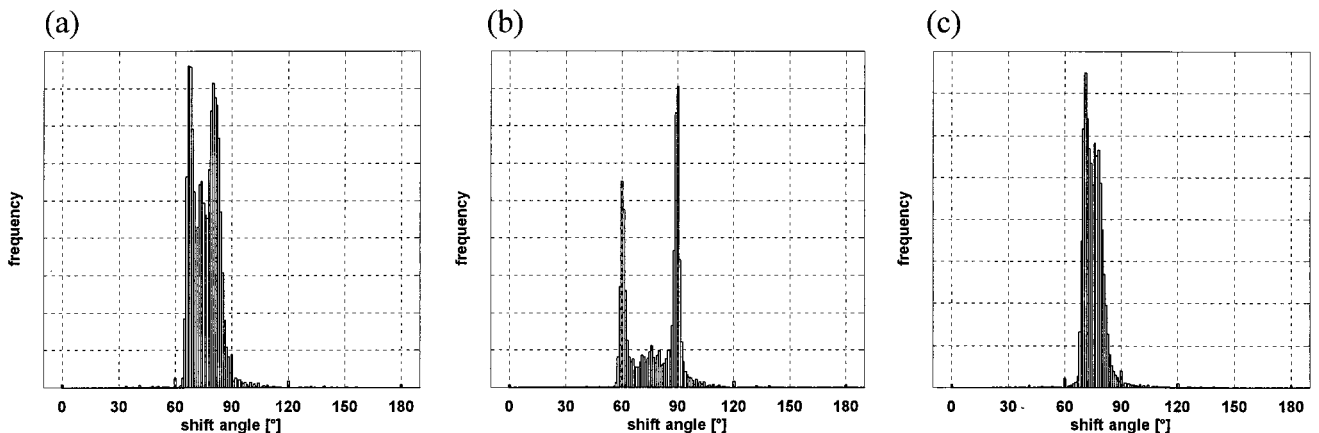

Fig. 9. Histograms for the fringe patterns used in Fig. 8.

Table 2. Shift-Angle Calculation by Several Methods for Simulated Fringe Patterns with Higher Harmonics[a]

Parameter and Method	Simulation 1	Simulation 2	Simulation 3	Simulation 4	Simulation 1	Simulation 2	Simulation 3	Simulation 4
α	72°	72°	72°	72°	45°	45°	45°	45°
σ_k	2.0	0.7	0.5	0.03	2.0	0.7	0.5	0.03
α calculated by COG ($M > 0$)	75.6°	74.0°	72.9°	72.0°	45.0°	39.0°	42.5°	45.1°
α calculated by COG ($M < 0$)	75.5°	74.0°	72.9°	72.0°	45.2°	39.0°	42.6°	45.1°
α calculated by lattice site with maximum frequency	120.0°	84.78°	67.98°	72.0°	60.0°	54.8°	49.8°	44.1°
α calculated by maximum histogram value	90°	82°	70°	72°	60°	55°	50°	45°
Mean value of $\alpha(x, y)$ within the measurement field	78.3°	76.5°	74.4°	72.1°	56.1°	47.1°	40.2°	45.7°

[a]Data for the simulation with Eq. (7): $Q = 10$, $I_0 = 127$, $\sigma_I = 3$, and γ varies from 0.55 to 0.95.

positive values of Z and M. The solid line represents a shift angle of $\alpha = 60°$. It contains 254 lattice sites (with possible integer values of Z and M). As this representation is point symmetric to the origin, there are 510 possible combinations of Z and M that yield $\alpha = 60°$ if the origin is not counted.

If we now reduce Z by 1, we obtain a shift angle of 60.13°, which is the closest possible value to 60°. The line for this value contains only two lattice sites besides the origin, i.e., [510, 254] and [−510, −254]; thus $\alpha = 60.13°$ is only twofold degenerate. Continuing this consideration for all possible values of α, we can explain the big difference in the degree of degeneracy of adjacent shift angles.

The cause of isolated peaks in the histogram is now obvious from the lattice-site representation. The frequency of the shift angles counted within the measurement field depends on the cut length of a line that represents a shift angle α with tails and cores and the number of lattice sites on this line (level of degeneracy). A low SNR causes an increase of the widths ω

(Fig. 3) of tail and core, while the cores move to the origin. The cut length between the highly populated cores and lines of highly degenerate shift angles (e.g., 60°, 90°, and 120°) increases, thus increasing the frequency of the corresponding shift angle in the histogram.

G. Influence of Higher Harmonics

Figures 8 and 9 show a series of lattice-site representations and the corresponding shift angle histograms for simulated Ronchi gratings [Figs. 8(a) and 8(b) and 9(a) and 9(b)] and for a Ronchi grating in a projected fringe application [Figs. 8(c) and 9(c)].

For an increasing influence of higher harmonics in the fringes the tail becomes curved until the lines for 60° and 90° have the highest population, which can also be seen in the corresponding histograms. The S-shaped structure is typical for the existence of higher harmonics in the fringes and can therefore be used to identify this kind of error source in an application. Depending on the actual shift angle, the lattice sites
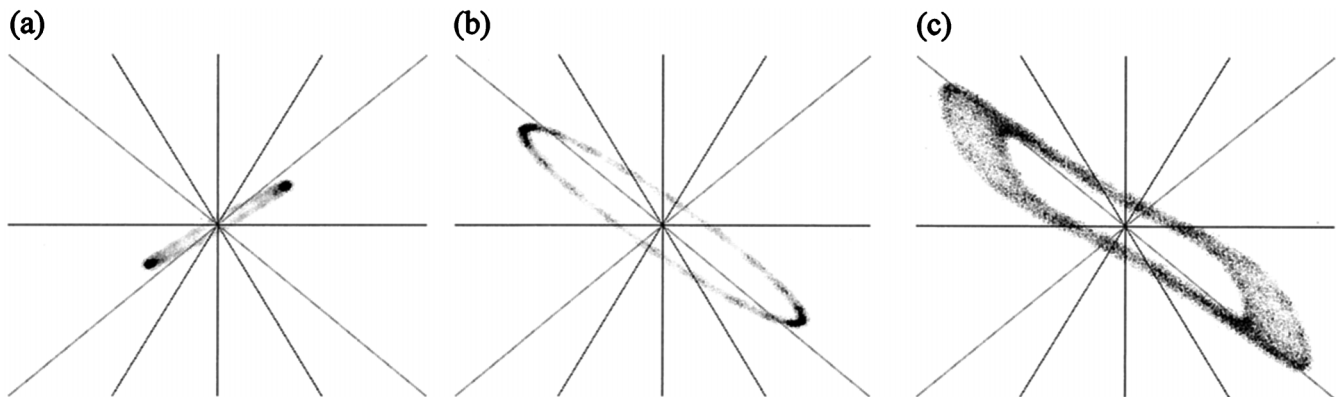

(a)   **(b)**   **(c)**

Fig. 10. Influence of a nonconstant shift angle on cores and tails in the lattice-site representation. Data for the simulation from Eq. (7): (a) Sinusoidal fringes, $I_0 = 60$, $\gamma = 0.75$, $\sigma_I = 3$, $Q = 0$, and statistical shift errors of $\alpha = [75.0°, 71.3°, 71.8°, 56.0°]$; (b) sinusoidal fringes, $I_0 = 127$, $\gamma = 0.75$, $\sigma_I = 3$, $Q = 0$, and systematic shift errors of $\alpha = [96.0°, 109.0°, 121.5°, 134.0°]$; and (c) Ronchi grating, $Q = 10$, and $\sigma_k = 0.7$ [for other data see (b)].
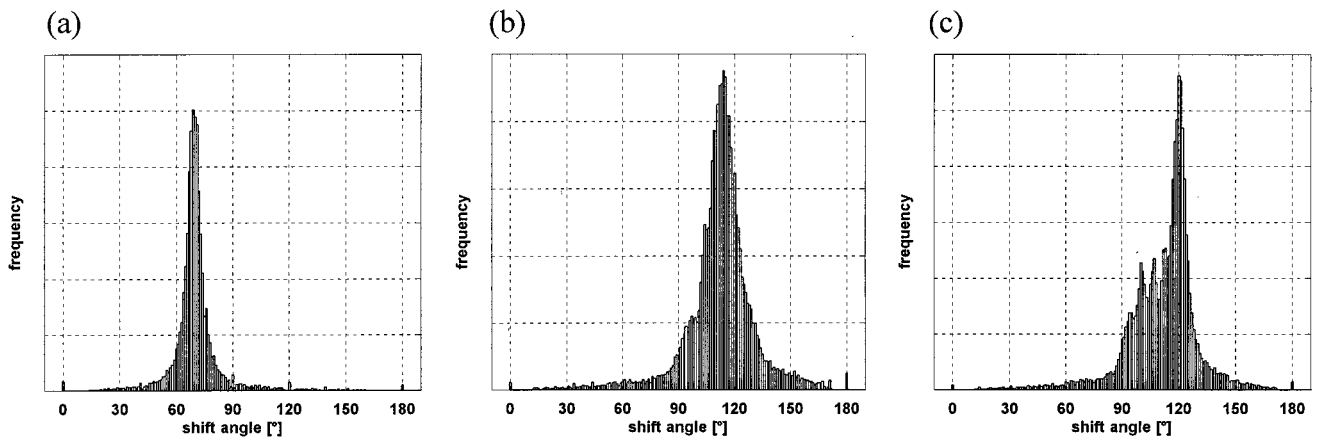
Fig. 11. Histograms for the fringe patterns used in Fig. 10.

tend toward a higher population of a pair of highly degenerate shift-angle lines [e.g., (60°, 90°) or (90°, 120°)]. The corresponding shift angle, however, can still be calculated with sufficient accuracy by the COG method, whereas other methods yield more inaccurate results or fail completely (Table 2). In many cases even the mean value of $\alpha(x, y)$ shows large deviations, as the spread of $\alpha(x, y)$ is no longer symmetric. Note that, for nonsinusoidal fringes shifted by 60°, 90°, or 120°, the S shape does not occur because all values already populate these highly degenerate lines.

H. Influence of a Nonconstant Shift Angle

Figures 9 and 10 show how the lattice-site representation and the shape of the histogram are influenced by a phase shift with a nonconstant shift angle. Nonconstant shift angles can be caused by statistical and systematic errors of the shifting device. Whereas statistical errors are often due to mechanical problems and have to be removed at more technical expense, systematic errors are often due to nonlinearities, which can be compensated for, e.g., by the controller of the shifting device.

In both cases, applying the COG method leads to results that represent the average value of the shift angles between the frames. It is of more importance, however, to identify these errors to remove them. Even for large deviations from the average shift angle, the histogram shows almost no deformation [Figs. 11(a) and 11(b)], whereas the lattice-site representation reveals a split of the tail (Fig. 10). This split is typical for shift errors and offers a possibility for identifying errors of this kind in an application.

As the typical shapes of tail and core for nonsinusoidal fringes are already known from our discussion above, we simulated a Ronchi grating with a systematic shift error. As can be seen from Fig. 10(c), both error types can be identified in the lattice-site repre-

sentation, which shows both tail splitting and an S shape.

3. Conclusion

The lattice-site representation of shift angles calculated by Eq. (2) provides a tool for accurate evaluation of the phase shift between fringe patterns by the COG method. In contrast to the evaluation of the histogram of shift angles, it is barely susceptible to deformation of the frequency distribution, caused, e.g., by degeneration of discrete shift-angle values or deviations of the fringe pattern from the ideal sinusoidal shape. The results of the COG method provide even more accuracy than the mean value of $\alpha(x, y)$. Furthermore, the lattice-site representation supplies a tool for identification of error sources (i.e., low SNR, nonlinear phase shifts, and insufficient defocusing of rectangular fringes) by the shape of tails and cores. This investigation still lacks a theoretical background, but experiments have clearly shown that the effects are not restricted to simulated fringe patterns.

References

1. D. Malacara, ed., *Optical Shop Testing*, 2nd ed. (Wiley, New York, 1992).
2. D. W. Robinson and G. T. Reid, eds., *Interferogram Analysis* (Institute of Physics, Bristol, UK, 1993).
3. K. Hibino, B. F. Oreb, D. I. Farrant, and K. G. Larkin, "Phase shifting of non-sinusodial wave-forms with phase-shift errors," J. Opt. Soc. Am. A **12,** 761–768 (1995).
4. J. Schwider, R. Burow, K. E. Elssner, J. Grzanna, R. Spolaczyk, and K. Merkel, "Digital wave-front measuring interferometry: some systematic error sources," Appl. Opt. **22,** 3421–3432 (1983).
5. K. Creath, "Phase-measurement interferometry techniques," in *Progress in Optics*, E. Wolf, ed. (Elsevier, Amsterdam, 1988), Vol. XXVI, pp. 349–393.